# Magneto-optical analysis of stripe elements embedded in a synthetic antiferromagnet

M. Langer,[1,2,*] A. Neudert,[1,†] J. I. Mönch,[3] R. Mattheis,[4] K. Lenz,[1] J. Fassbender,[1,2] and J. McCord[5,1]

[1]*Institute of Ion Beam Physics and Materials Research, Helmholtz-Zentrum Dresden-Rossendorf, Bautzner Landstr. 400, 01328 Dresden, Germany*[‡]

[2]*Technical University Dresden, 01069 Dresden, Germany*

[3]*Institute for Integrative Nanosciences, IFW Dresden, 01069 Dresden, Germany*

[4]*Leibniz Institute of Photonic Technology (IPHT), 07745 Jena, Germany*

[5]*Institute of Materials Science, University of Kiel, 24143 Kiel, Germany*

(Received 3 September 2013; revised manuscript received 21 December 2013; published 14 February 2014)

Domain structures and the magnetic reversals of micrometer stripe patterns embedded in a weakly antiferromagnetically exchange coupled $Co_{90}Fe_{10}$/Ru/$Co_{90}Fe_{10}$ trilayer were investigated. Patterning was achieved by means of ion irradiation through a lithographically defined mask. In this process, irradiated parts become ferromagnetic due to interfacial intermixing. The embedded stripes fabricated by this technique are compared to stripes patterned by reactive ion etching. Using magneto-optical Kerr microscopy, the domain structure and the shape of the magnetic reversal for both kinds of stripes have been studied. Observed differences in the switching behavior are explained by modifications of the magnetic material properties, e.g., anisotropy and saturation magnetization due to the ion irradiation. Irradiated 2-μm-wide stripes show a collective switching with quasidomains during the magnetic reversal. This observation indicates interactions of the internal magnetization of embedded stripes with the adjacent ones in the nonirradiated antiferromagnetically coupled trilayers. Two possible mechanisms suspected to mediate these interactions are discussed: a deviation of the antiparallel magnetic orientation in the synthetic antiferromagnetic material leading to an effective magnetic moment, as well as a domain wall at the boundary of two different kinds of stripes. The latter investigation is supported by micromagnetic simulations.

DOI: 10.1103/PhysRevB.89.064411 PACS number(s): 75.30.Gw, 75.50.Cc, 75.60.Ch

## I. INTRODUCTION

Magnetic patterning on a micro- and nanometer scale is of highest interest for potential applications such as XMR sensors [1,2] or bit patterned media for data storage applications [3–6]. Besides, periodic magnetic structures are in demand for latest research, e.g., as magnonic crystals in the fast ascending field of magnonics [7,8]. For this purpose, ion irradiation can be employed providing several advantages compared to conventional patterning techniques such as reactive ion etching (RIE). One is the possibility to locally modify magnetic properties without multistep deposition processes using multiple materials. In the past, stripe patterning by ion irradiation was applied to modify several magnetic properties such as exchange bias [9–13], coercive field [13,14], magnetic anisotropy [9,15–17], and saturation magnetization [7,9,18–20]. The latter can be diminished until the area, which is exposed to the ion beam, becomes magnetically dead [14,21]. This results in a periodic ferromagnetic (FM) stripe array, where FM stripes are embedded in a nonmagnetic matrix.

To create similar structures, the use of antiferromagnetically (AF) interlayer exchange coupled trilayers, referred to as synthetic antiferromagnets (SAFs), offers the opportunity to obtain magnetically similar structures with strongly reduced ion irradiation fluence. In these systems, ion irradiation is used to locally erase the coupling between both magnetic layers and thus, create embedded ferromagnetic elements [as depicted in Fig. 1(b)] in a quasi-nonmagnetic (SAF) environment. The fluence needed to cause direct exchange coupling in an SAF is less than the one needed to erase ferromagnetism in a full magnetic thin film of the same thickness. Note that with the lower fluence regime, surface sputtering is also significantly reduced. Hence, the element boundaries are *magnetic property*

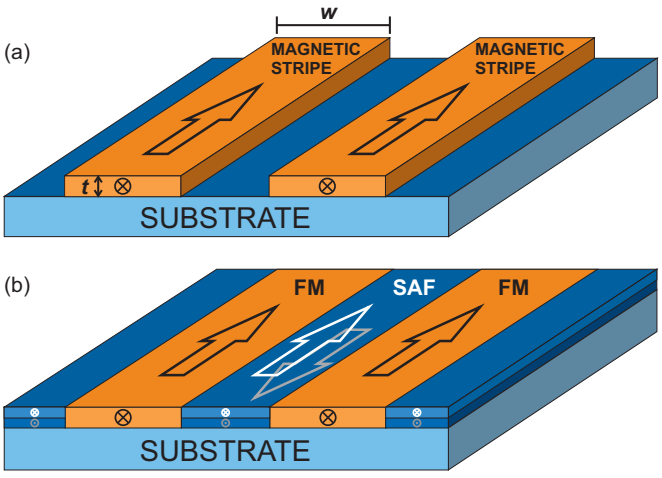


FIG. 1. (Color online) Structure of the two analyzed stripe patterns: (a) FM stripes created by RIE and sitting on top of the substrate and (b) FM stripes fabricated by exposing an SAF to a $Co^+$ ion beam. Orange color identifies the actual FM $Co_{90}Fe_{10}$ stripes, whereas different shades of blue represent either the $Si/SiO_2$ substrate or the SAF consisting of two antiparallel coupled $Co_{90}Fe_{10}$ layers separated by a Ru spacer. Arrows mark the local magnetization direction.

*Corresponding author: manuel.langer@hzdr.de

†Present address: Fraunhofer Institut für Photonische Mikrosysteme, 01109 Dresden, Germany

‡http://www.hzdr.de/fwin

 

borders but not *structural* borders and the stray field between the irradiated structures is reduced due to the shielding of the surrounding magnetic material.

In previous works, the interactions of embedded square elements in a strong interlayer exchange coupled SAF have been investigated using an Fe/Cr/Fe trilayer system with a fourfold anisotropy [22,23]. Therein, analytical calculations [23] are presented as explanation for the observed interaction between several square elements. In the energetic considerations, two magnetic states are discussed, an array of squares with internal Landau structure separated by an SAF in the antiparallel state and one global Landau structure across the whole array, in which the magnetization of both SAF layers is pointing in the same direction.

The present work returns to a less complex uniaxial system. Instead of a two-dimensional pattern, a one-dimensional extended array of micrometer-size stripes embedded in a weakly coupled $Co_{90}Fe_{10}$/Ru/$Co_{90}Fe_{10}$ SAF, was chosen. The aim is to study and understand the lateral interactions of embedded stripe elements considering the idea that an opening of the antiparallel aligned magnetization in the SAF causes an effective magnetic moment mediating an interaction. In addition, a domain wall at the boundary of embedded stripes is analyzed using micromagnetic simulations. The behavior of this system [depicted in Fig. 1(b)] is compared to an array of isolated $Co_{90}Fe_{10}$ stripes with the same dimensions [see Fig. 1(a)].

The paper is organized as follows. The particular technique of combining UV lithography with ion irradiation on an SAF as well as the precharacterization of the magnetic material modified by ion irradiation can be found in Sec. II. The results are presented in Sec. III, which is divided into two parts, namely the Kerr microscopy analysis of stripes with a nominal width of $w = 20\,\mu$m and $2\,\mu$m, respectively. The latter contains a detailed discussion of the observed stripe-stripe interaction. Finally, in Sec. IV, it will be concluded that the observed interaction is most likely caused by the residual magnetic moment of the SAF.

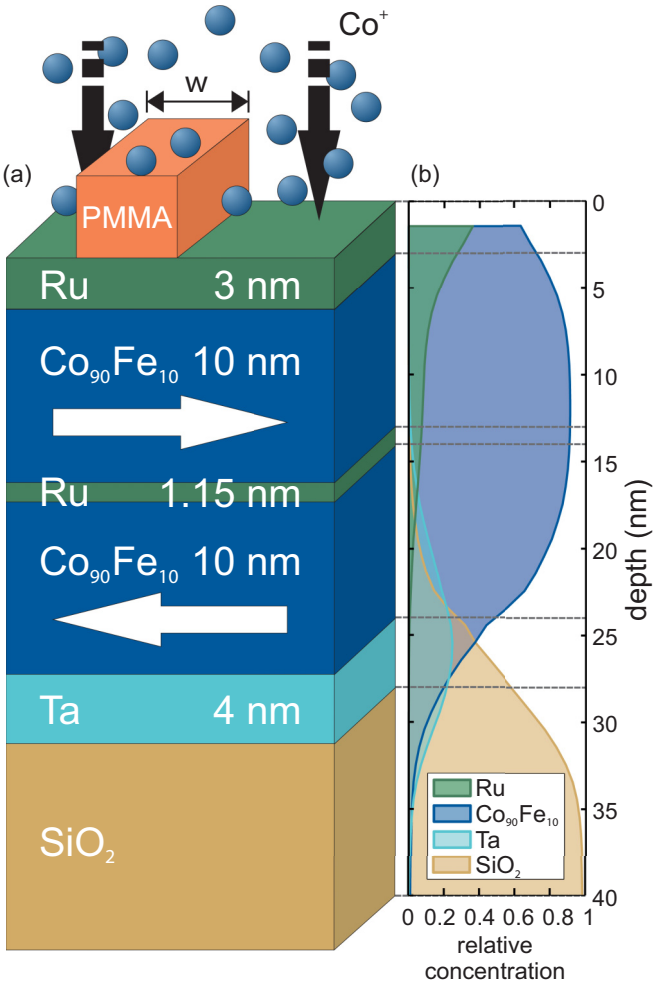


FIG. 2. (Color online) (a) Sketch of the layer structure for the embedded magnetic elements before ion irradiation. (b) Depth-dependent concentration profile after ion irradiation with 80-keV $Co^+$ ions at a fluence of $5 \times 10^{15}$ $Co^+/cm^2$, calculated using TRIDYN.

## II. EXPERIMENTAL DETAILS

### A. Sample fabrication

The full stack of the $Co_{90}Fe_{10}$/Ru/$Co_{90}Fe_{10}$ SAF was dc sputtered using a UHV system (base pressure $\leqslant 2 \times 10^{-8}$ mbar) and is depicted schematically in Fig. 2(a). A 4-nm Ta buffer layer deposited on the Si/$SiO_2$ substrate serves as seed layer. The SAF itself consists of two 10-nm $Co_{90}Fe_{10}$ layers separated by a 1.15-nm-thin Ru spacer. The thickness of the Ru was preselected in order to obtain a moderate AF coupling. This has several advantages, such as the low saturation field, which allows to measure the full hysteresis of the stack with relatively low magnetic fields accessible in the magneto-optical Kerr effect (MOKE) setups. During the deposition, the sample is moved nearly linearly with respect to the targets causing a uniaxial in-plane anisotropy with easy axis along the moving direction. For the purpose of protection against oxidation and to suppress the sputter etch of the magnetic layers during low dose ion irradiation, a 3-nm Ru cap layer was added. In order to obtain the stripe pattern, a 2-μm-thick polymethylmethacrylate (PMMA) mask was applied using UV lithography acting as a template for the ion irradiation. $Co^+$ ions were used to intermix the nonmagnetic Ru interlayer in order to preserve the stoichiometry of $Co_{90}Fe_{10}$. The resulting stack behaves like one magnetic single layer.

Simulations using the SRIM [24] (the stopping and range of ions in matter) package were carried out to determine the optimal ion energy. For different energies, calculations of the depth-dependent distribution of the collision effects during the irradiation have been performed. The results indicate that for an ion energy of 80 keV the mean penetration depth of the ions matches the depth of the interlayer.

To find the suitable irradiation fluence, an analysis of several reference samples irradiated in a range of $1\times10^{13}$–$1\times10^{16}$ $Co^+/cm^2$ was performed. On the one hand, the sample should show a clear FM behavior (meaning an almost Stoner-Wohlfarth-like shape of the magnetic reversal), which is improving with increasing fluence. On the other hand, the saturation magnetization $M_S$ and the uniaxial anisotropy constant $K_u$ were desired to be as high as possible but are decreasing with increasing fluence. The finally selected irradiation fluence

TABLE I. Magnetic properties of the trilayer stack before and after ion irradiation.

| | $M_S$ (G) | $H_K$ (Oe) | $K_u$ ($10^3$ erg/cm$^3$) | $J_1$ (erg/cm$^2$) |
|---|---|---|---|---|
| nonirradiated | 1560 [29] | 18.2 | 14.2 | −0.181 |
| irradiated | 1090 | 7.7 | 4.2 | . . . |

of $F = 5 \times 10^{15}$ Co$^+$/cm$^2$ was an appropriate compromise between all the desired magnetic properties (values given in Table I).

For this fluence, TRIDYN [25,26] simulations shown in Fig. 2(b) exhibit a strong intermixing of the interlayer with the adjacent $Co_{90}Fe_{10}$. According to the results, the interlayer is fully intermixed and there is only one magnetic single film remaining. After the irradiation, the magnetic material shows a depth-dependent distribution that indicates a gradient in $M_S$ [27]. Thus, one would expect a strongly reduced $M_S$ in the top and the bottom of the magnetic layer compared to the central part due to the different concentrations of $Co_{90}Fe_{10}$. In the following, the magnetic layer will be treated like a homogeneous thin film with an effectively reduced $M_S$ since further investigations of the depth-dependent saturation magnetization are no objective of this work.

Systematic investigations of a nonirradiated $Co_{90}Fe_{10}$ wafer revealed a homogeneous alignment of the anisotropy axis with an angular deviation of only $\pm 3^\circ$. However, narrowly confined spots were found where the anisotropy direction shows a local deviation of up to $\pm 15^\circ$. Nevertheless, the irradiated samples show generally deviations of $\pm 15^\circ$. Thus, contributions to this anisotropy rotation caused by the ion irradiation are probable.

In order to compare the magnetic behavior of such free-standing stripes fabricated by ion beam patterning, a layer composition equivalent to the initial film system of the embedded stripes [see Fig. 2(a)] was used. Basically, this $SiO_2$/Ta (4 nm)/$Co_{90}Fe_{10}$ (20 nm)/Ru (3 nm) structure equals the afore mentioned AF coupled trilayers if the Ru interlayer is neglected. By RIE, this stack was etched down to the substrate to fabricate stripe patterns of the same dimensions as in case of the embedded ones. Both kinds of stripes are schematically depicted in Fig. 1.

Symmetric stripe patterns (nominal widths of irradiated and nonirradiated stripes are equal) in a range of $w = 2$–$20$ μm were investigated. However, AFM measurements (not shown) have proven that the 2-μm FM stripes have an actual structural width of 2.5 μm, whereas the nonirradiated stripes are 1.5-μm wide. The same effect also occurs for the 20-μm stripes but not in case of the etched stripes. Deviations of the structural width of patterns using UV lithography and RIE have already been investigated elsewhere [28]. In the following, the samples will be referred by the nominal stripe width. Besides, the existence of a transition zone at the element's boundaries is highly probable. In this zone, properties change gradually due to proximity effects, such as scattering underneath the resist mask.

### B. Magnetic precharacterization

To determine the impact of ion irradiation on several magnetic material parameters such as $K_u$ and $M_S$, a preinvestigation was carried out. Therefore, the hysteresis loops of unpatterned $Co_{90}Fe_{10}$ single films and SAFs before and after ion irradiation were measured using vibrating sample magnetometry (VSM) and MOKE magnetometry. The results are depicted in Fig. 3. By fitting the hard axis loops, $K_u$ and the coupling strength $J_1$, shown in Table I, were determined.

The magnetic reversals of the nonirradiated SAF are shown in Fig. 3(a). The loops have a shape typical for weakly coupled, symmetric SAFs with the characteristic three step hysteresis in the easy axis measurement. In contrast, the loops of an irradiated SAF in Fig. 3(b) exhibit a typical ferromagnetic behavior with the linear shape of the hard axis measurement (in red) and the rectangular shape in case of the easy axis measurement (black curve). Moreover, both loops ensure an approximately constant magnetization of the SAF in the field range of the full magnetic reversal of the irradiated FM thin film. This is important for the switching behavior of embedded stripes since they are desired to switch separately from their neighboring SAF ones.

Furthermore, inductive loop measurements (not shown here) revealed a significant reduction of $M_S$ after the ion irradiation. All material properties gained by these measurements are summarized in Table I.

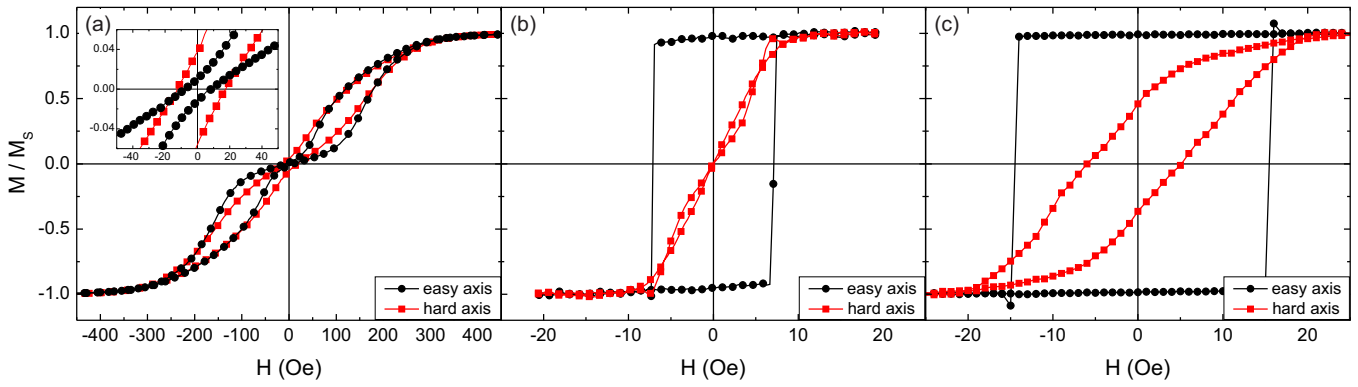


FIG. 3. (Color online) (a) VSM hysteresis curve of an extended antiferromagnetically coupled $Co_{90}Fe_{10}$ trilayer as deposited and (b) after ion irradiation (MOKE measurement). For comparison, (c) shows the Kerr loops of a nonirradiated 20-nm $Co_{90}Fe_{10}$ single film. (b) and (c) represent the unpatterned magnetic material of the embedded and the etched stripes, respectively.

Moreover, the magnetic reversal of a nonirradiated 20-nm $Co_{90}Fe_{10}$ single film was measured in easy and hard directions by MOKE magnetometry [see Fig. 3(c)]. In comparison to this single layer, the irradiated $Co_{90}Fe_{10}$ trilayer stack [see Fig. 3(b)] exhibits a major decrease of the anisotropy field $H_K$ and the saturation magnetization $M_S$ (both values are given in Table I) due to irradiation effects [30,31]. Thus, the value of the uniaxial anisotropy constant $K_u = 1/2\, H_K M_S$ is strongly reduced compared to the value before ion irradiation. For the micromagnetic analysis of the two types of stripe patterns, Kerr microscopy and high-resolution MOKE magnetometry were used.

## III. RESULTS

### A. 20-µm-wide stripes

At first, 20-µm-wide stripes with anisotropy oriented parallel to the stripe axis are investigated. During the field sweep along the stripe axis, the Kerr images of both systems—embedded as well as etched stripes—reveal a fast motion of a 180° head-to-head domain wall (shown in Fig. 4). The main difference is the much higher switching field in case of the etched elements.

The measurement perpendicular to the stripe axis (see Fig. 5) shows a vastly increased complexity. In case of the etched stripes, inhomogeneous ripplelike domain structures appear [see Fig. 5(a)], which grow by a combination of rotational processes and wall movements towards a state beyond zero field of almost antiparallel alignment of the magnetization inside different domains. The Kerr images Figs. 5(b) and 5(c) show domains with magnetization almost

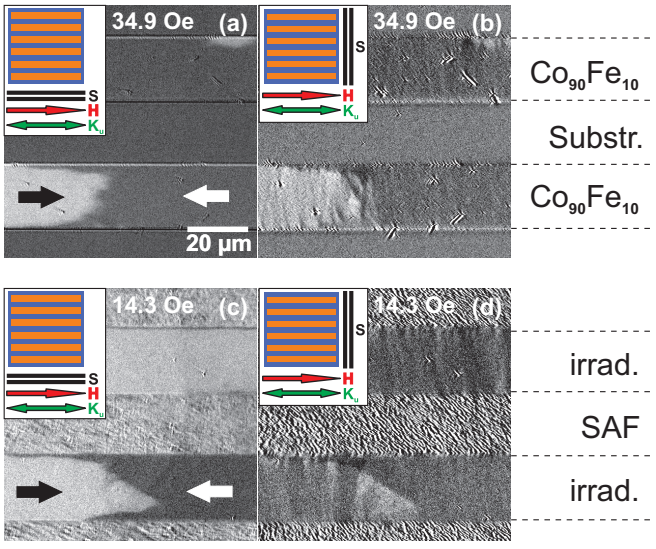


FIG. 4. (Color online) Kerr images of a domain wall crossing the 20-µm-wide stripes during magnetic hysteresis with field aligned parallel to the stripe axis. Both images in one row show different magnetic sensitivities of the same magnetic state. The stripes displayed on top are etched ones (a) and (b). Embedded ones can be found on the bottom (c) and (d). (a) and (c) depict a longitudinal magnetic contrast, whereas (b) and (d) show the transversal one. The small insets on the top left of each image indicate the orientation of external field $H$, anisotropy $K_u$, and magnetic sensitivity $S$.

pointing in opposite directions separated by 180° walls. Applying a small counterfield (15–25 Oe) leads to a stepwise destruction of the 180° walls and an ongoing rotation of the stripe-internal magnetization with increasing counter field [see Figs. 5(c) and 5(d)]. Through the whole process of the magnetic reversal, narrow domains pinned at the elements edge can be identified. The high demagnetizing field at the boundaries forces the local magnetization in an orientation parallel to the stripe axis. Thus, these domains are very stable and similar to edge curling walls [32].

The magnetic reversal of the embedded stripes shows a different behavior [see Figs. 5(k)–5(t)]. As the field is increased starting from negative saturation, the magnetization rotates collectively away from the short stripe axis until, at zero field, it almost uniformly aligns parallel to the stripes [see Figs. 5(l) and 5(q)]. In Figs. 5(m) and 5(r), one can see ripples evolving in the center of the stripe at a field of 13.2 Oe. They gradually evolve with increasing field towards a central domain where the magnetization has a major component parallel to the stripe axis but opposite to the one at the stripe boundary [depicted in Figs. 5(n) and 5(s)]. This domain nucleation is a consequence of the major differences of the demagnetizing field between the stripe edge and its center. Further increase of the field, as depicted in Figs. 5(o) and 5(t), leads to a complete rotation of the magnetization in the central domain into the field direction. Only within a few micrometers at the boundary, the magnetization remains with a significant component parallel to the stripe edges. This observation is identical to the one studied before in reference [32] and is referred to as edge curling wall. It is a stable edge domain magnetized parallel to the stripe axis and exists only at high fields while the center of the stripe is already saturated.

To explain the differences in the switching behavior, the demagnetizing field needs to be estimated. For this purpose, assuming noninteracting stripes, the analytical formula of Brown for the ballistic demagnetizing field $H_D'^B$ of an infinitely long cuboid oriented along the $y$ direction with a cross section of $(t \times w)$ was used [33]:

$$H_D'^B = 4\pi D_z' M_S, \tag{1}$$

where

$$\pi D_z' = 2 \arctan\left(\frac{2t}{w}\right) - \frac{w}{2t}\ln\left(1 + \frac{4t^2}{w^2}\right) \tag{2}$$

with $D_z'$ being the demagnetizing factor of the stripes along the $z$ direction. The width $w$ and thickness $t$ are sketched in Fig. 1. The values of the measured effective anisotropy $H_{K,eff}^{meas}$ determined by fitting hard axis loops in Fig. 6 gained from high-resolution MOKE magnetometry as well as the semi-theoretical values $H_{K,eff}^{theor}$ can be found in Table II. $H_{K,eff}^{theor}$ denotes the sum of the measured uniaxial anisotropy field $H_K = 2K_u/M_S$ (values for $K_u$ and $M_S$ can be found in Table I) and the demagnetizing field $H_D'^B$ calculated from Eq. (1):

$$H_{K,eff}^{theor} = 4\pi D_z' M_S + 2K_u/M_S. \tag{3}$$

In case of 20-µm stripe width, the values $H_{K,eff}^{meas}$ and $H_{K,eff}^{theor}$ are in a good agreement in spite of the fact that the AF-coupled magnetic environment surrounding the embedded stripes is neglected in Eq. (3) (its net magnetic moment is close to zero).

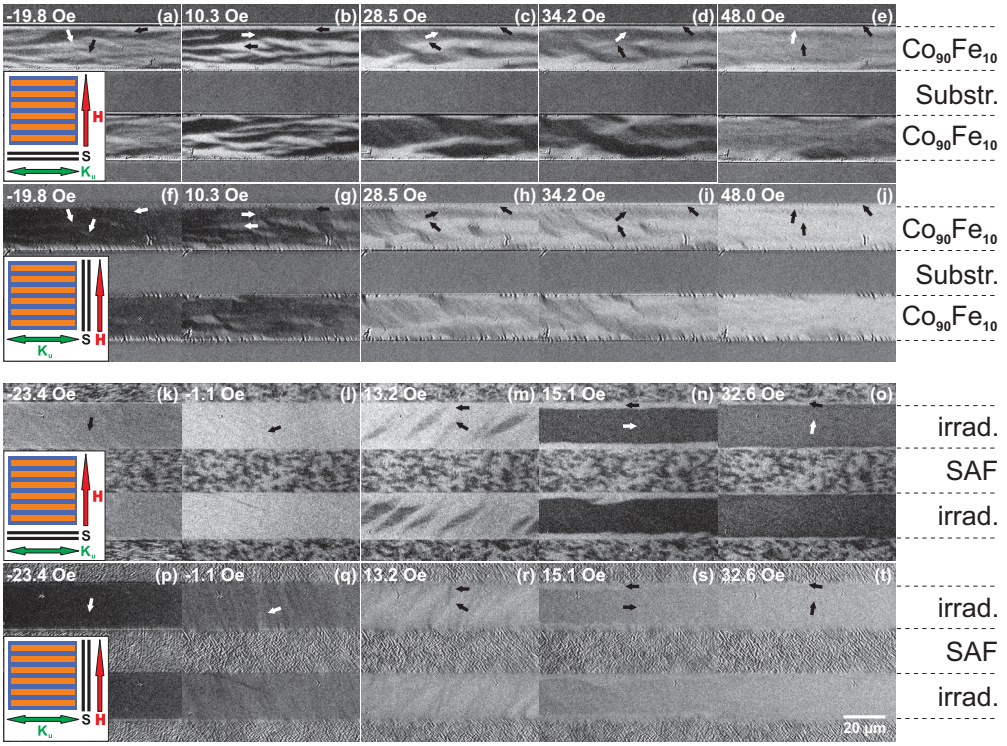


FIG. 5. (Color online) Kerr microscopy images showing the magnetic reversal of patterns of 20-µm-wide stripes, which are fabricated (a)–(j) by etching and (k)–(t) by ion irradiation, respectively. The external field was applied perpendicular to the stripe axis, which is indicated by the sketches at the bottom left showing the directions of the external magnetic field $H$, the anisotropy $K_u$, and the magnetic sensitivity $S$ with respect to the orientation of the stripes. Corresponding Kerr images in one column depict the longitudinal and the transversal contrast of the identical magnetic state, respectively.

Thus, major differences in the switching behavior can be explained by the effects of ion irradiation, such as the reduction of the intrinsic anisotropy field. Together with the decrease of $M_S$, both govern the differences in the domain formations during the magnetic reversal. In both kinds of stripes, a formation of edge domains appears, which in both cases, can be explained by the high demagnetizing field at the boundary. Besides, in case of the embedded stripes, the proximity of the neighboring SAF stripes implies the existence of a domain wall at the edge (the domain wall will be discussed more detailed in Sec. IIIB2 for the 2-µm stripes), which acts also as a pinning center for edge domains with magnetization pointing parallel to the stripes. One main difference, the magnetization in the center of the stripe showing an extended domain for embedded stripes [see Fig. 5(n)] and a pattern of antiparallel magnetized domains for etched stripes [see Fig. 5(c)], can be explained by the strength of the intrinsic anisotropy. If $K_u$ is small, the central magnetization of the stripe is governed by the Zeeman energy and orients uniformly towards the direction of the external field. Whereas in the center of etched stripes,

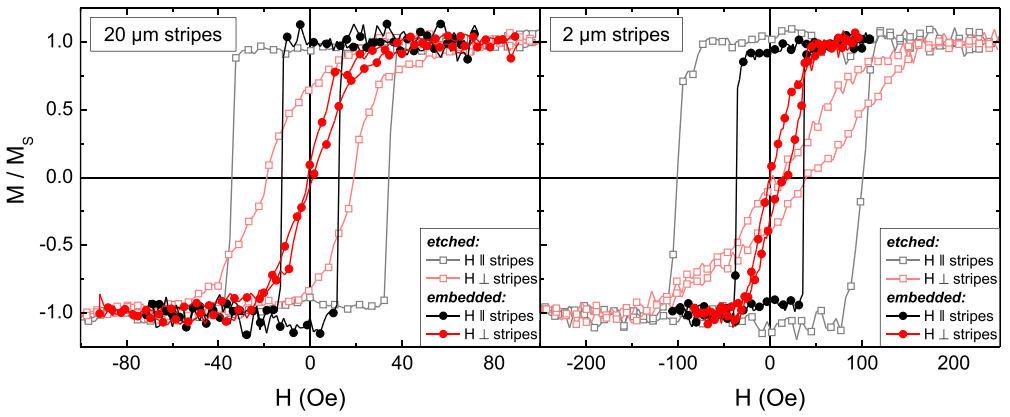


FIG. 6. (Color online) High-resolution MOKE magnetometry hysteresis loops of 20-µm and 2-µm stripes, etched and embedded, measured with external field direction parallel and perpendicular to the stripes. The hard axis loops were fitted to extract the values of the measured anisotropy constant $H_{K,eff}^{meas}$ specified in Table II.

TABLE II. Comparison of experimental and theoretically estimated values of the effective anisotropy.

| | etched | | irradiated | |
|---|---|---|---|---|
| width (μm) | 20 | 2 | 20 | 2 |
| $H_{K,eff}^{meas}$ (Oe) | 40(20)[a] | 140(21) | 19(3) | 38(6) |
| $H_D^{/B}$ (Oe) | 12.5 | 124.8 | 8.7 | 69.8[b] |
| $H_{K,eff}^{theor}$ (Oe) | 37(5) | 150(5) | 16(1) | 78(1) |

[a]The uncertainty is due to a nonlinear shape of the hard axis loop (shown in Fig. 6), which can be observed in extended polycrystalline $Co_{90}Fe_{10}$ thin films as well [cf. Fig. 3(c)].
[b]A stripe width of 2.5 μm was used for the calculation of this value due to a broadening of the irradiated stripes (see text).

Zeeman energy and anisotropy energy govern the alignment of magnetization leading to complex domain patterns with antiparallel oriented domains at zero field, shown in Figs. 5(b) and 5(g). Increasing the external field, magnetization rotates by wall motions and rotary processes towards the field direction [depicted in Figs. 5(e) and 5(f)].

### B. 2-μm-wide stripes

#### 1. *Magneto-optical analysis*

Figure 7 shows Kerr images during the switching process of 2-μm-wide stripes, while the external field is applied along the stripe axis. In Figs. 7(a) and 7(b), the uniaxial anisotropy is also parallel to the stripes, whereas it is perpendicular to them in Figs. 7(c) and 7(d). The switching fields are similar for both orientations of the anisotropy axis. The coercive field, $H_c$, of the etched stripes is approximately 100 Oe and single stripes switch independently from their neighbors [see Figs. 7(a) and 7(c)]. In case of the embedded stripes, a much lower $H_c$ of approximately 35 Oe was measured and several stripes switch collectively with distinct stripe-crossing quasi domains [see Figs. 7(b) and 7(d)]. This observation reveals a stripe-stripe interaction, which was observed before in other works dealing with stripe patterns fabricated by ion irradiation [10,12,18,19,34]. Independent from its direction, the rather low intrinsic anisotropy is suppressed by the high shape anisotropy.

For a quantitative description, estimations of the demagnetizing field according to Eq. (3) were made. The results are also given in Table II. In case of the etched 2-μm stripes, there is a good agreement of the measured effective anisotropy field (estimated from the hard axis loops illustrated in Fig. 6) to the semitheoretical one. This is not the case for the embedded 2-μm stripes, which will be discussed below.

The stripes in Fig. 7(d) behave clearly like an effective medium with domain borders crossing several FM and SAF stripes. However, most domain boundaries are still given by the edges of the stripes in case of Fig. 7(b). Hence, the intensity of the interaction between several stripes seems to be stronger for perpendicular alignment of the intrinsic anisotropy than for parallel orientation. For a firm understanding of these differences in the switching, the transversal magnetization component has been visualized during the magnetic reversal along the stripe axis. In Fig. 8(a), the intrinsic anisotropy

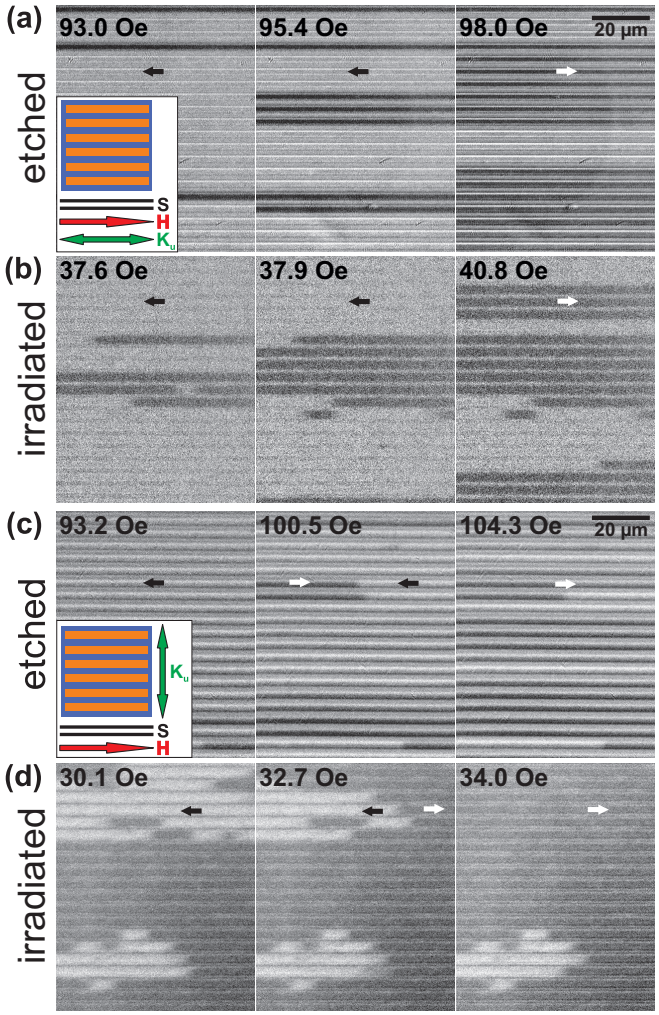


FIG. 7. (Color online) Kerr microscopy images of 2-μm-wide stripe patterns, which were prepared (a) and (c) by etching and (b) and (d) by ion irradiation. For the upper rows (a) and (b), the uniaxial anisotropy lies parallel to the stripes, whereas it is perpendicular in (c) and (d). The insets depict the orientations just as in Fig. 5.

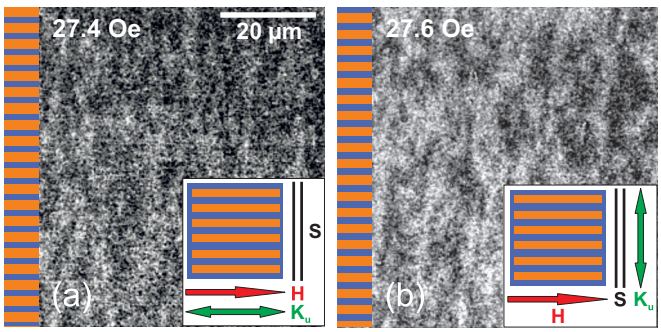


FIG. 8. (Color online) Kerr microscopy images of ion irradiated 2-μm-wide stripe patterns. The magnetic sensitivity is adjusted in a way that the transverse magnetization causes the contrast in the pictures. In (a), the anisotropy is parallel to the stripes, whereas in (b), it is perpendicular. Orange and violet colored stripes denote the irradiated and nonirradiated stripes whereas the symbols at the bottom right mark directions equivalent to Fig. 5.

is parallel to the stripe axis whereas in Fig. 8(b) it is perpendicular. In both cases, a patch pattern is visible, which extends over the whole image. This pattern is similar to the typical patch patterns observable in AF coupled trilayers [35]. In our case, however, these patches also exist in the FM stripes. Another peculiarity of both images in Fig. 8 is that the Kerr contrast of these transversal patch domains is higher for perpendicular alignment [see Fig. 8(b)] than for parallel orientation [see Fig. 8(a)]. Together with the observed quasidomains in Figs. 7(b) and 7(d), this indicates a correlation between the strength of the stripe-stripe interaction and the scale of the transversal magnetization component.

### 2. *Analysis of the interaction between embedded stripes*

In this section, the lateral interaction of 2-μm embedded stripes is investigated. Therefore, two mechanisms are analyzed as possible origin. One explanation for the stripe-stripe interaction would be a domain wall located at the boundaries between both kinds of stripes, the SAF and the FM ones. As already shown in previous work [18,19], such interaction can exist, if the stripe width $w$ is in the same dimension as the width $\delta$ of the domain walls (including their long extended tails) between irradiated and nonirradiated stripes. Another mechanism suspected to mediate the observed transaction is the partial breaking of the AF coupling due to the high effective field acting on the 2-μm SAF stripes. The coercive field of the 2-μm embedded stripes ($H_C^{2\,\mu m} \cong 35$ Oe) is more than twice as high compared to the 20-μm stripes ($H_C^{20\,\mu m} \cong 14$ Oe). Due to the weak interlayer exchange coupling strength of the SAF, the magnetic moments of both layers are no longer aligned fully antiparallel and hence, an additional effective magnetic moment is generated in the SAF stripes.

In order to estimate the structure and size of the domain wall at each stripe edge, micromagnetic simulations[1] [36] based on the Landau-Lifschitz-Gilbert equation [37,38] were performed. The used material parameters for both kinds of stripes are given in Table I. Moreover, the exchange stiffness constant $A$ was assumed to be $2 \times 10^{-6}$ erg/cm for the irradiated as well as the nonirradiated parts [39]. The vertical architecture in case of the SAF stripe consisted of two 10-nm-thick $Co_{90}Fe_{10}$ thin films separated by a nonmagnetic 1-nm spacer. In case of the irradiated stripe, a full 21-nm $Co_{90}Fe_{10}$ thin film (with reduced $M_S$ and $K_u$) was assumed. Equal to a full period of the 2-μm stripe pattern, 4000 nm have been chosen as the width of the simulated structure. The cell size was selected to be 8 nm × 8 nm × 5 nm in both magnetic layers and 8 nm × 8 nm × 1 nm in the interlayer. Laterally, periodic boundary conditions were used to reproduce the periodicity of the 2-μm stripe pattern in $x$ direction and to simulate an infinite extension of the stripes in $y$ direction. Initially, all spins were saturated along the $y$ axis and relaxation was carried out without an external magnetic field. The results for the anisotropy orientation either parallel or perpendicular to the stripes are illustrated in Fig. 9. Here, the normalized magnetization components in top and bottom layers are shown.

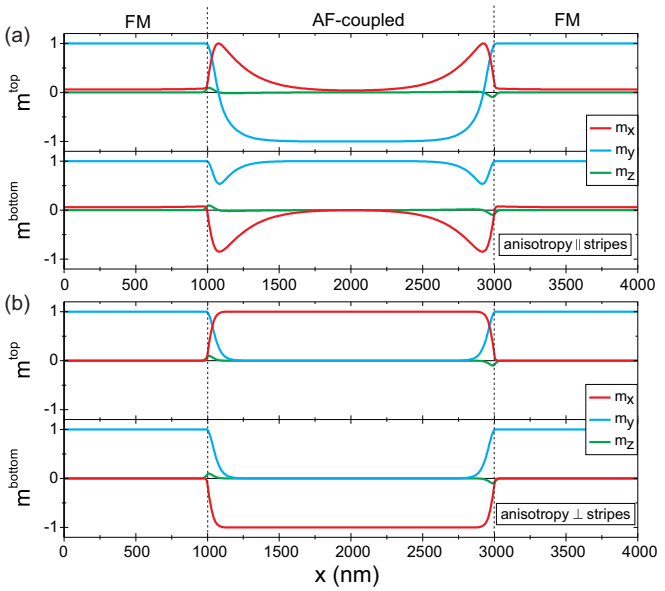


FIG. 9. (Color online) Micromagnetic simulations of the domain wall configuration in a periodic pattern of 2-μm-wide stripes for the top and the bottom layer. In (a), the anisotropy axis is parallel to the stripes, whereas in (b), both are oriented perpendicular to each other.

For a parallel alignment of anisotropy and stripe axis [see Fig. 9(a)], the simulation shows a wide 180° domain wall ($\delta = 289$ nm) right at the edges of the stripes with an extended tail reaching into the SAF stripe. In the case of a perpendicular orientation [Fig. 9(b)] of the anisotropy, a rather small 90° domain wall ($\delta = 84$ nm) is established. The aforementioned integral domain wall widths $\delta$ were calculated using the following definitions:

$$\delta = \int m_x \, dx, \quad 180^\circ \text{ wall}, \tag{4}$$

$$\delta = 2 \int m_x \, m_y \, dx, \quad 90^\circ \text{ wall}. \tag{5}$$

As boundaries for the integration, the middle of each stripe, SAF and FM, was selected. However, the resulting domain walls contradict the observed intensity of the stripe interactions, which were stronger for a perpendicular than for a parallel anisotropy. The calculations above would predict in fact the opposite: a stronger interaction for the parallel case compared to the perpendicular one due to the determined size of the domain walls. An essential factor, i.e. the misalignment of the local anisotropy (suspected to cause the observed characteristic patch pattern [35], see Fig. 8), was not considered in the micromagnetic simulations. Furthermore, a misalignment of the internal anisotropy due to its directional uncertainty discussed in Sec. II, was neglected. Likewise, a transition zone at the border of SAF and FM stripes, where magnetic properties change continuously, was not taken into account.[2]

[1] LLG Micromagnetics Simulator 2.50.

[2] Properties in the micromagnetic model were assumed to change discontinuously neglecting any transition zone at the stripes boundaries.

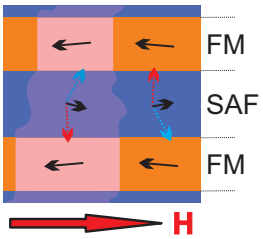


FIG. 10. (Color online) Sketch of the stripe-stripe interaction driven by a small effective magnetic moment in the SAF stripes, due to a partially breaking of the AF coupling. The stripe pattern is illustrated close to the coercive field of the FM stripes with patch domains visible in transversal sensitivity.

Thus, the reality, involving patch domains in the SAF stripes, could not be reproduced and the resulting shapes of the domain walls remain questionable.

In contrast, a stripe-stripe interaction can be caused by an effective magnetic moment in the SAF stripes due to the presence of an external field. With increasing effective field, the angle $\alpha$ between the two magnetization orientations of top and bottom layer becomes smaller. This implies the existence of a net magnetic moment in the nonirradiated 2-µm stripes. Figure 10 depicts the slight opening of the angle $\alpha$ between top (red arrow) and bottom (blue arrow) layer inside the AF coupled stripes causing an effective magnetic moment (black arrow), which interacts with the neighboring FM stripes.

Using the easy axis loop in Fig. 3(a), the effective magnetic moment of the SAF stripes can be estimated. At a counter field equal to the mean switching field of the 2-µm stripes (approximately 35 Oe), an effective magnetic moment of $3.1\%M_S$ was measured. Note that the same measurement shows an effective moment of $0.4\%M_S$ in remanence.

Since these values refer to an extended SAF, the effective magnetic moment of 2-µm narrow stripes can be even higher due the integration over many magnetic domains in the SAF and the presence of the adjacent FM stripes. The extended tail of the domain wall at the boundaries leads to an decreasing of $\alpha$ towards the stripe borders. Besides, the simulation of the irradiated stack in Fig. 2 indicates that after irradiation, the left over magnetic moment is not anymore distributed exactly symmetric to the position of the Ru interlayer of the nonirradiated SAF. The consequence of all points above would be a stronger two-way interaction between SAF and embedded stripes than estimated above. Hence, the $3.1\%M_S$ can be understood as a minimal appraisal value. Due to the high length-width aspect ratio, the stray field contribution of the embedded FM stripes can be neglected as long as they are assumed to be magnetized parallel to the stripe edge.

The net moment of the SAF stripes neighboring to the FM ones causes an additional internal field, which is a likely explanation for the switching of FM stripes at lower external fields, than expected from Eq. (3) (see Table II). Equation (2) is no longer applicable since the stripes were assumed to be magnetically isolated and noninteracting. Moreover, the typical patch pattern stands in connection with slight deviations of the local anisotropy in SAFs [35] similar to the origin of magnetization ripple in single layers. The occurrence of similar domain structures in the transversal sensitivity (depicted in Fig. 8) crossing SAF-stripes as well as FM ones is a major evidence that the stripe-stripe interaction is governed by this mechanism.

High-resolution MOKE magnetometry was used to measure the hysteresis loops of 2-µm-wide SAF stripes and to determine the correlation between them and their neighboring FM stripes. Figure 11(a) illustrates the results for AF coupled stripes with the anisotropy parallel to the stripe axis. Figure 11(b) shows those with a perpendicular alignment. The jumps in the latter are the main differences compared to the loops in case of a parallel anisotropy orientation. They occur at field values around $\pm 30$ Oe, which corresponds to the $H_C$ of the FM stripes confirming a strong interaction between both kinds of stripes. Whereas in case of a parallel anisotropy [see Fig. 11(a)] at field values around $\pm 30$ Oe the slope of the loop is much smoother compared to the distinctive jump in Fig. 11(b). The field values of these jumps confirm the supposed hypothesis of Sec. IIIB, which reveals that the significantly stronger lateral coupling for stripes with a perpendicular anisotropy is governed by an effective net magnetic moment in the SAF stripes.

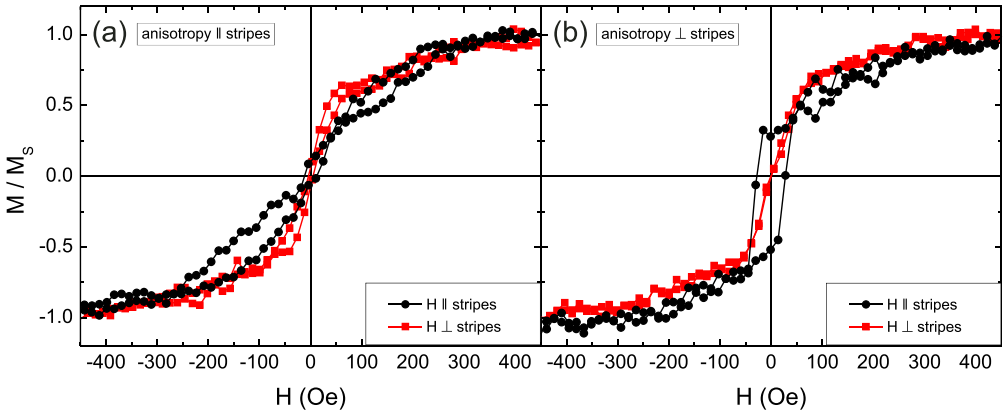


FIG. 11. (Color online) Hysteresis loops of 2-µm SAF stripes measured by high-resolution MOKE magnetometry. In (a), the anisotropy axis is oriented parallel to the stripes, whereas in (b), it is perpendicular to them. Thus, (a) shows the hysteresis of the SAF stripes shown in Fig. 7(b) whereas (b) corresponds to those illustrated in Fig. 7(d).

## IV. CONCLUSION

Ion irradiation has been successfully applied to create a lateral pattern of embedded ferromagnetic stripes in a synthetic antiferromagnet. Kerr microscopy investigations of the switching behavior of embedded and etched stripes of the same dimensions were performed. Calculations of the theoretical effective anisotropy field ($H_{K,\mathrm{eff}}^{\mathrm{theor}}$) based on the estimation of the average demagnetizing field are in a good agreement with the experimentally measured values of large 20-μm stripes. Differences in the switching behavior of embedded stripes compared to etched stripes could be explained by the modification of the magnetic material properties, such as $M_S$ and $K_u$ due to the ion irradiation. For smaller stripes of 2-μm width, extended quasidomains were observed during the magnetic reversal and it was shown that they act as an effective medium together with the antiferromagnetically coupled stripes. A magnetic net moment in the synthetic antiferromagnetic stripes is likely to be the origin of this interaction. Transversal measurements showing a patch pattern typical for extended synthetic antiferromagnets as well as measurements of the hystereses of antiferromagnetically coupled stripes support this thesis.

To increase the density of independently switchable embedded elements fabricated by similar techniques, the use of synthetic antiferromagnets with a stronger interlayer exchange coupling is recommended. Higher coupling fields guarantee the elimination of the effective magnetic moment of the antiferromagnetically coupled stripes, which is believed to be crucial for the stripe-stripe interaction.

## ACKNOWLEDGMENTS

The authors thank J. Osten, R. Neb, and T. Strache for the fruitful discussions as well as M. Körner for his assistance with the micromagnetic simulations. This work is supported by the Deutsche Forschungsgemeinschaft (Grants FA314/3-2 and MC9/7-2).

[1] M. Diegel, S. Glathe, R. Mattheis, M. Scherzinger, and E. Halder, IEEE Trans. Magn. **45**, 3792 (2009).
[2] J. Fassbender, S. Poppe, T. Mewes, J. Juraszek, B. Hillebrands, K.-U. Barholz, R. Mattheis, D. Engel, M. Jung, H. Schmoranzer, and A. Ehresmann, Appl. Phys. A **77**, 51 (2003).
[3] B. C. Stipe, T. C. Strand, C. C. Poon, H. Balamane, T. D. Boone, J. A. Katine, J.-L. Li, V. Rawat, H. Nemoto, A. Hirotsune, O. Hellwig, R. Ruiz, E. Dobisz, D. S. Kercher, N. Robertson, T. R. Albrecht, and B. D. Terris, Nat. Photon. **4**, 484 (2010).
[4] S. Xiao, X. Yang, S. Park, D. Weller, and T. P. Russell, Adv. Mater. **21**, 2516 (2009).
[5] R. Ruiz, H. Kang, F. A. Detcheverry, E. Dobisz, D. S. Kercher, T. R. Albrecht, J. J. de Pablo, and P. F. Nealey, Science **321**, 936 (2008).
[6] S. Sun, C. B. Murray, D. Weller, L. Folks, and A. Moser, Science **287**, 1989 (2000).
[7] I. Barsukov, F. M. Römer, R. Meckenstock, K. Lenz, J. Lindner, S. Hemken to Krax, A. Banholzer, M. Körner, J. Grebing, J. Fassbender, and M. Farle, Phys. Rev. B **84**, 140410(R) (2011).
[8] J. Ding, M. Kostylev, and A. O. Adeyeye, Phys. Rev. B **84**, 054425 (2011).
[9] J. Fassbender and J. McCord, J. Magn. Magn. Mater. **320**, 579 (2008).
[10] K. Theis-Bröhl, A. Westphalen, H. Zabel, U. Rücker, J. McCord, V. Höink, J. Schmalhorst, G. Reiss, T. Weis, D. Engel, A. Ehresmann, and B. P. Toperverg, New J. Phys. **10**, 093021 (2008).
[11] K. Theis-Bröhl, M. Wolff, A. Westphalen, H. Zabel, J. McCord, V. Höink, J. Schmalhorst, G. Reiss, T. Weis, D. Engel, A. Ehresmann, U. Rücker, and B. P. Toperverg, Phys. Rev. B **73**, 174408 (2006).
[12] J. McCord, R. Schäfer, K. Theis-Bröhl, H. Zabel, J. Schmalhorst, V. Hoink, H. Bruckl, T. Weis, D. Engel, and A. Ehresmann, J. Appl. Phys. **97**, 10K102 (2005).
[13] J. McCord, T. Strache, I. Mönch, R. Mattheis, and J. Fassbender, Phys. Rev. B **83**, 224407 (2011).
[14] C. Chappert, H. Bernas, J. Ferré, V. Kottler, J.-P. Jamet, Y. Chen, E. Cambril, T. Devolder, F. Rousseaux, V. Mathet, and H. Launois, Science **280**, 1919 (1998).
[15] N. Martin, J. McCord, A. Gerber, T. Strache, T. Gemming, I. Mönch, N. Farag, R. Schäfer, J. Fassbender, E. Quandt, and L. Schultz, Appl. Phys. Lett. **94**, 062506 (2009).
[16] J. McCord, I. Mönch, J. Fassbender, A. Gerber, and E. Quandt, J. Phys. D: Appl. Phys. **42**, 055006 (2009).
[17] S. C. Shin, S. K. Han, J. Hong, and S. Kang, Appl. Phys. Express **4**, 116501 (2011).
[18] J. McCord, L. Schultz, and J. Fassbender, Adv. Mater. **20**, 2090 (2008).
[19] J. Fassbender, T. Strache, M. O. Liedke, D. Markó, S. Wintz, K. Lenz, A. Keller, S. Facsko, I. Mönch, and J. McCord, New J. Phys. **11**, 125002 (2009).
[20] D. McGrouther, J. N. Chapman, and F. W. M. Vanhelmont, J. Appl. Phys. **95**, 7772 (2004).
[21] D. McGrouther, W. A. P. Nicholson, J. N. Chapman, and S. McVitie, J. Phys. D: Appl. Phys. **38**, 3348 (2005).
[22] R. Neb, T. Sebastian, P. Pirro, B. Hillebrands, S. Pofahl, R. Schäfer, and B. Reuscher, Appl. Phys. Lett. **101**, 112406 (2012).
[23] S. Blomeier, B. Hillebrands, B. Reuscher, A. Brodyanski, M. Kopnarski, and R. L. Stamps, Phys. Rev. B **77**, 094405 (2008).
[24] J. Biersack and L. Haggmark, Nucl. Instrum. Methods Phys. Res., Sect. B **174**, 257 (1980).
[25] W. Möller and W. Eckstein, Nucl. Instrum. Methods Phys. Res., Sect. B **2**, 814 (1984).
[26] W. Möller, W. Eckstein, and J. Biersack, Comput. Phys. Commun. **51**, 355 (1988).
[27] D. Markó, K. Lenz, T. Strache, R. Kaltofen, and J. Fassbender, IEEE Trans. Magn. **46**, 1711 (2010).
[28] C. Hamann, I. Mönch, R. Kaltofen, R. Schäfer, T. Gemming, L. Schultz, and J. McCord, J. Appl. Phys. **104**, 013926 (2008).
[29] C. Hamann, Master's thesis, IFW Dresden, 2005.
[30] J. Fassbender and J. McCord, Appl. Phys. Lett. **88**, 252501 (2006).

[31] J. Fassbender, A. Mücklich, K. Potzger, and W. Möller, Nucl. Instrum. Methods Phys. Res., Sect. B **248**, 343 (2006).
[32] R. Mattheis, K. Ramstock, and J. McCord, IEEE Trans. Magn. **33**, 3993 (1997).
[33] J. W. F. Brown, in *Magnetostatic Principles in Ferromagnetism, Appendix*, edited by E. P. Wohlfarth (North-Holland, Amsterdam, 1962).
[34] K. Theis-Bröhl, C. Hamann, J. McCord, B. P. Toperverg, and H. Zabel, J. Phys.: Conf. Ser. **211**, 012014 (2010).
[35] M. Rührig, R. Schäfer, A. Hubert, R. Mosler, J. A. Wolf, S. Demokritov, and P. Grünberg, Phys. Status Solidi A **125**, 635 (1991).
[36] M. R. Scheinfein, J. Unguris, J. L. Blue, K. J. Coakley, D. T. Pierce, R. J. Celotta, and P. J. Ryan, Phys. Rev. B **43**, 3395 (1991).
[37] L. Landau and E. Lifshitz, Phys. Z. Sowjetunion **8**, 153 (1935).
[38] T. L. Gilbert, IEEE Trans. Magn. **40**, 3443 (2004).
[39] D. V. Berkov and N. L. Gorn, Phys. Rev. B **80**, 064409 (2009).